Improved control effect of absence seizures by autaptic connections to the subthalamic nucleus

Denggui Fan[1,2] and Qingyun Wang[3]

[1]*School of Mathematics and Physics, University of Science and Technology Beijing, Beijing 100083, China*

[2]*Beijing Key Laboratory of Knowledge Engineering for Materials Science, Beijing 100083, China*

[3]*Department of Dynamics and Control, Beihang University, Beijing 100191, China*

(Received 19 June 2018; published 28 November 2018)

We presently propose a modified basal ganglia–corticothalamic (MBGCT) mean-field network of neural populations by incorporating the autaptic connection to subthalamic nucleus (STN) (termed ACS). The network connection is through the pulse field generated by the incoming pulse rate from the prepopulation, which is functioned into postpopulation. And then, we study the control effect of STN deep brain stimulation (DBS) on epileptic absence seizures characterized by 2–4 Hz spike and wave discharges (SWD) as the modulation of ACS is applied. For the slow dynamical effect of STN on cortical seizure activity, DBS electrodes are employed to generate sustaining input pulse of electrical potential field. In particular, the continuous symmetrical and asymmetrical charge-balanced biphasic pulse DBS with interphase gap, i.e., S-CBBP-IPGx and AS-CBBP-IPGx stimulations, are used due to their less charge and multiply adjustable stimulation parameters, to evaluate their effect on the suppression of SWD occurrence. Based on the percentage of control for the SWD number, it is shown that strong ACS directly contributes to the abatement of SWD. In contrast, weak ACS can significantly improve the control effects of CBBP DBS, which are particularly dependent on the stimulation shapes; i.e., (i) AS-CBBP-IPGx is less beneficial than S-CBBP-IPGx, (ii) CBBP DBS in frequency-dependent manner can bidirectionally modulate the SWD occurrence, and (iii) CBBP DBS with moderate interphase gap (IPG) is more effective to suppress the SWD occurrence than that with no or large IPGs. These results are basically consistent with the experimental findings, which computationally supports the involvement of STN in the control mechanism of epileptic absence seizures.

DOI: 10.1103/PhysRevE.98.052414

I. INTRODUCTION

Absence seizures are characterized by bilaterally synchronized and well structured ∼2–4 Hz spike and wave discharges (SWD) in the electroencephalogram (EEG) observations of absence epilepsy [1–3]. The main clinic manifestation of absence seizures is the transient and sudden deprivation of consciousness [4]. It is believed that SWD is the reflection of the abnormally synchronous oscillations in the corticothalamic (CT) loop. In particular, experimental findings have suggested the pacemaker role of thalamic reticular nucleus (RE) in initiating SWD during seizure process [5–8]. In addition, accumulating evidences show that the basal ganglia (BG) is involved in the controlling of the SWD [9–13]. Thus, basal ganglia-corticothalamic circuit (BGCT) has been prevailingly hypothesized to play a major role in the modulation of absence seizures. It also provides a framework to understand the role of these circuits in modulating the generalized seizures. Accordingly, most theorists base the generations and modulations of SWD on the BGCT circuit.

Epileptic seizures that appear and disappear almost instantly are intermittent periods of the brain's activity. Therefore, the interruption of the normal activity may be due to bistable dynamics consisting of background state and seizure rhythm [14–17]. In such a scenario, seizures can be induced or stopped, in theory at least, by a single counterpulse delivered at the right instances. In addition to the bistability, epileptic seizure rhythms can also be induced from background activity by a change of parameter to a pathological value, i.e., crossing a bifurcation point [15,18]. However, these two situations are uniformly down to the parameter changes but due to the random fluctuations of parameters on a fast and slow timescale, respectively. In particular, this parameter disturbance could be caused by the change of mutual interaction (e.g., coupling strength) between various nuclei within the cortex, cortex-thalamus, or cortex–basal ganglia–thalamus circuits. In fact, there is accumulating evidence that absence epilepsy is highly associated with the abnormal interactions between the cerebral cortex and thalamus. Besides the direct coupling, anatomical evidence also suggests the key roles of the basal ganglia in the modulation of absence seizures. Therefore, in this paper, based on the BGCT circuit model we will outline the bifurcation curves between the various dynamical states using the interactive function parameters and shape the parametric region of seizures.

The biophysically realistic mean-field model, which was proposed to study the macroscopic dynamics of neural populations in a simple yet efficient way, is used to describe the population dynamics of the BGCT circuit. In this circuit, each neural population gives rise to a field of pulses, which travels to other neural population at a mean conduction velocity. The network connection is through the pulse field generated by the incoming pulse rate from the prepopulation which is functioned into postpopulation. The network framework of this model is inspired by recent modelling studies [10,11], which is shown schematically in Fig. 1. As seen from Fig. 1, BGCT

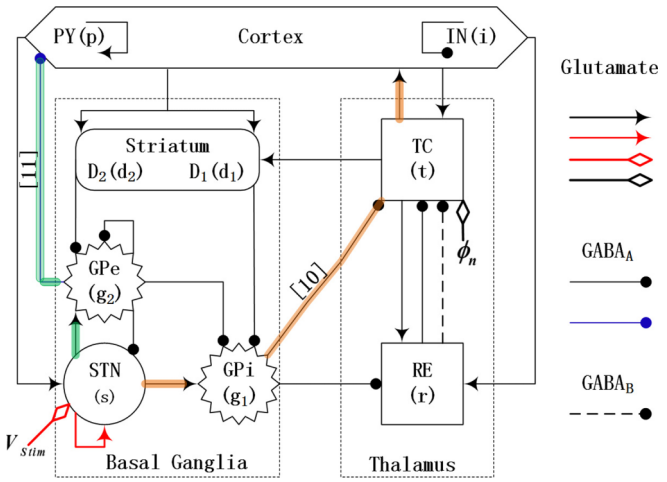

FIG. 1. Schematic of the modified basal ganglia–corticothalamic (MBGCT) model with the introduction of autaptic connections to subthalamic nucleus (STN), indicated by the red arrow. The other connectivity of MBGCT network is the same as that of the original BGCT model [10,11]. That is, the arrows depict the glutamate-mediated excitatory synapses. The solid and dashed lines with filled circles represent the $GABA_A$- and $GABA_B$-mediated inhibitory projections, respectively. The framework of MBGCT model network is composed of cortical subnetwork, thalamic subnetwork and the subnetwork of basal ganglia. p-excitatory pyramidal neurons (PY) and i-inhibitory interneurons (IN) belong to cortical subnetwork; r-thalamic reticular nucleus (RE) and t-specific relay nuclei (TC) belong to thalamic subnetwork; and the basal ganglia subnetwork consists of d_1-striatal D1 neurons, d_2-striatal D2 neurons, g_1-globus pallidus internal (GPi) segment, g_2-globus pallidus external (GPe) segment, and s-subthalamic nucleus (STN). ϕ_n denotes the nonspecific background noise entering the TC neuronal populations. V_{stim} indicates the external electrical stimulation input. The brown [10] and green [11] shade lines represent the potential forward and backward projection pathways from STN to cortex.

circuit consists of three modules: (1) cortex, which is composed of excitatory pyramidal neuronal populations (PY, p) and inhibitory interneuronal populations (IN, i); (2) thalamus, which comprises the thalamic reticular nucleus (RE, r) and specific relay nuclei (TC, t); and (3) basal ganglia including striatal neurons $D_1/D_2(d_1/d_2)$, globus pallidus interna and externa segments (GPi/GPe, g_1/g_2) and subthalamic nucleus (STN, s). Based on the works conducted by Chen *et al.* [10,11], these nine neuronal populations are anatomically and topologically connected through three types of neural projections. The solid lines with circle head and arrows represent the $GABA_A$ mediated inhibitory projections and glutamate mediated excitatory projections, respectively. The dashed line denotes the $GABA_B$ mediated inhibitory projection with a transmission delay due to the relatively slow kinetics. In addition, TC receives a nonspecific external input indicated by ϕ_n. In addition to the interconnections between various neuronal populations within BGCT, as shown in Fig. 1, self-connection, known as autapses meaning a synaptic connection from a neuron onto itself, is also very common in neuronal networks [19–22]. For example, the self-synaptic dynamics of PY, IN, and GPe have been introduced into the BGCT network dynamics. Also, in the reduced corticothalamic loop model, Guo *et al.* [22] investigated the effect of self-inhibition of RE neurons on the seizure suppressions. In fact, autapses has been found from pyramidal neurons [23,24] of cat visual cortex and the developing rat neocortex, more commonly from the inhibitory neurons [25,26]. The self-stimulating nature of autapses may offer the effective approach or economical method to affect neuronal activity dynamics and control network dynamics toward specific states. However, in the BGCT circuit, besides the existed several types of self-synaptic functions, the self-excitation of STN has never been involved in the seizure dynamics. It might also offer insights into regulating absence seizures. Motivated by this, STN self-excitation will be considered in this paper as shown with the red arrow in Fig. 1. We thereby propose a modified BGCT (MBGCT) network (see Fig. 1).

Deep brain stimulation (DBS) has been developed for the surgical approach of neurological disorders [27–35]. In particular, clinical evidences have also suggested that STN DBS could be a promising treatment for patients with drug-resistant epilepsy who would not benefit from conventional surgery [36]. More importantly, past experimental and computational studies have shown that applying suitable DBS to STN can inhibit the production of SWD during absence seizures [13,27,37,38]. As shown in the work of Suffczynski *et al.* [14], bistability can be present in the thalamic network without input from the cortex, the cortical network without thalamic involvement, as well as the thalamo-cortical circuit network [16]. However, basal ganglia was not shown to be directly involved in the bistability of basal ganglia-corticothalamic circuit. Therefore, the modulation of basal ganglia for the cortical seizure activity may involve in the parameter fluctuation between corticothalamic circuit and basal ganglia on the slow timescale. This also suggests that when the stimulation is set on basal ganglia, e.g., STN, to activate STN, the single-pulse stimulation may not generate effect strong enough to affect the cortical seizure activities through upstream projections. Thus, the continuous long-lasting stimulations which can generate the accumulative effect may be the preferred choice to effectively affect the cortical seizures. In addition, experimental evidence also suggests the effect of continuous high-frequency on the seizure abatement [39–41]. In particular, Ref. [38] showed that bilateral 5-s high-frequency stimulations (130 Hz) of STN could suppress ongoing spontaneous absence seizures in rats and [13] analyzed the frequency-dependent effects of DBS in STN on SWD of absence seizure in tg mice. Therefore, in this paper, the control effect of STN-DBS with continuous electric input pulse on epileptic absence seizures is investigated.

However, it is difficult to optimize the DBS parameters for each specific patient, which is generally adopted by experimental or clinical experiences. In addition, it is reported that DBS cannot be equally effective for all the pathological symptoms and at all the time, due to the intrinsic complexity of epilepsy. The mechanism underlying the effects of DBS is still enigmatic and under debate. However, to obtain the desired curative effect, it is needed to constantly adjust the stimulation therapies and stimulation parameters. Besides the stimulation efficacy, how to extend battery life and potentially reduce the side effects should also be considered in designing the stimulus patterns. In light of this, in this paper we will

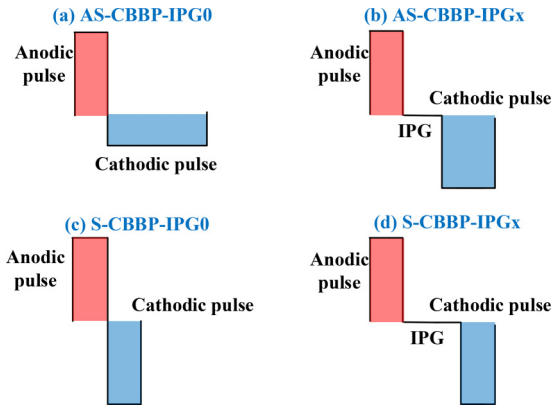

FIG. 2. Overview of four types of charge-balanced biphasic pulse deep brain stimulation (CBBP-DBS) with a leading phase (anodic pulse) and a lagging phase (cathodic pulse): (a) asymmetrical CBBP with no interphase gap (IPG) (AS-CBBP-IPG0), (b) AS-CBBP with IPG (AS-CBBP-IPGx), and symmetric CBBP without (c) or with (d) IPG (S-CBBP-IPG0 or S-CBBP-IPGx), respectively.

apply periodic charge-balanced biphasic pulse deep brain stimulation (CBBP-DBS) to STN. This stimulation pattern has the advantage of less charge and broad adjustable stimulation parameters [42]. As shown in Fig. 2, the asymmetrical and symmetrical CBBP-DBS with and without inter-phase gap, i.e., AS-CBBP-IPGx, AS-CBBP-IPG0, S-CBBP-IPGx, and S-CBBP-IPGx are mainly considered, respectively. The red line with rhombus in Fig. 1 indicates the applied DBS. However, research on DBS for epilepsy is actively pursuing multiple avenues simultaneously. Hence, in this paper, based on the MBGCT model we mainly investigate the comprehensive effects of autaptic connection to STN (ACS) and STN CBBP DBS on the SWD occurrence and suppression. Our aim is to computationally examine the involvement of STN in modulating epileptic absence seizures and provide the testable hypotheses for future clinical research.

II. MATHEMATICAL MODEL AND SETUP

A. Mathematical model of modified basal ganglia–corticothalamic (MBGCT) circuit

The dynamic of each nucleus within the MBGCT loop is described by the neurophysiologically relevant mean-field model of neural population [10,11,43–47]. The spatiotemporal mean firing rate $R_x(\mathbf{r},t)$ of neural populations can be estimated by their corresponding mean membrane potential $V_x(\mathbf{r},t)$ at the spatial position $\mathbf{r}$ and time t with the sigmoid function

$$R_x(\mathbf{r},t)=\Gamma[V_x(\mathbf{r},t)]=\frac{R_x^{\max}}{1+\exp\left[-\frac{\pi(V_x(\mathbf{r},t)-\Theta_x)}{\sqrt{3}\sigma_x}\right]}, \quad (1)$$

where $x\in\Lambda=\{p,i,d_1,d_2,g_1,g_2,s,r,t\}$, indicating the different neural populations, $R_x^{\max}$ represents the maximum firing rate. Following the previous works [10,11], $R_x^{\max}$ is set within the physiological parameter ranges, i.e., $R_p^{\max}=R_i^{\max}=R_{g_1}^{\max}=R_t^{\max}=R_r^{\max}=250$ Hz, $R_{d_1}^{\max}=R_{d_2}^{\max}=65$ Hz, $R_{g_2}^{\max}=300$ Hz, $R_s^{\max}=500$ Hz. Θ_x and σ_x are the threshold variables of mean firing rate. Here, $\Theta_p=\Theta_i=\Theta_t=\Theta_r=15$ mV, $\Theta_{d_1}=\Theta_{d_2}=19$ mV, $\Theta_{g_1}=\Theta_s=10$ mV, $\Theta_{g_2}=9$ mV, and $\sigma=6$ mV. The $V_x(\mathbf{r},t)$ is ulteriorly determined by the incoming postsynaptic potentials from other neuronal populations, which can be modeled as

$$D_{ab}V_x(\mathbf{r},t)=\sum_{y\in\Lambda}\upsilon_{xy}\phi_y(\mathbf{r},t). \quad (2)$$

Here, D_{ab} is a differential operator having the form

$$D_{ab}=\frac{1}{ab}\left[\frac{\partial^2}{\partial t^2}+(a+b)\frac{\partial}{\partial t}+ab\right], \quad (3)$$

which can represent the dendritic filtering of incoming signals. $\phi_y(\mathbf{r},t)$ is a field generated by the neural population y to represent the incoming pulse rate functioned into other neural populations. Note that ϕ_n=2 mVs is the nonspecific subthalamic input onto TC. υ_{xy} is the coupling strength from the neural population y to x. $a=50\,\mathrm{s}^{-1}$ and $b=200\,\mathrm{s}^{-1}$ are the decay and rise times of responses to incoming signals, respectively.

In particular, when the external stimulation is applied on STN, the potential of STN, $V_s(\mathbf{r},t)$, is determined by

$$D_{ab}V_s(\mathbf{r},t)=\sum_{y\in\Lambda}\upsilon_{sy}\phi_y(\mathbf{r},t)+\upsilon_s\phi_{\mathrm{DBS}}(\mathbf{r},t), \quad (4)$$

where $\phi_{\mathrm{DBS}}(\mathbf{r},t)$ is the input pulse of electrical field generated by the stimulation electrodes, i.e., the working electrode (WE) and counterelectrode (CE). υ_s is the intensity of stimulation electrical field having the unit of V.

A delay parameter τ is particularly considered in the incoming pulse rate of RE, i.e., $\phi_r(\mathbf{r},t-\tau)$, to describe its slow synaptic kinetics due to that GABA_B functions via second messenger processes. Following the previous setting, τ is scanned in [20,70] with the unit of ms. In addition, compared to other neural populations, the axons of cortical excitatory pyramidal neurons are sufficiently long to yield significant projection effects when ϕ_p travels to other neural populations. In our system, we assume the spatial activity is uniform because absence seizures are believed to occur simultaneously throughout the brain. Hence, the projection effect of ϕ_p is governed by

$$\frac{1}{\gamma_p^2}\left[\frac{\partial^2}{\partial t^2}+2\gamma_p\frac{\partial}{\partial t}+\gamma_p^2\right]\phi_p=R_p(t)=\Gamma[V_p], \quad (5)$$

where $\gamma_p=100$ Hz controls the temporal damping rate of cortical pulse. For the rest of the neural populations, the projection effect can be ignored due to the too short axons, which gives $\phi_z=\Gamma(V_z)=R_z(t), z\in\{i,d_1,d_2,g_1,g_2,s,r,t\}$. In particular, we assume $V_i=V_p$ and $R_i=R_p$ because of the fact that intracortical connectivities are proportional to the numbers of synapses involved.

Thus, according to the Eqs. (1)–(4) the MBGCT model with external electric stimulus applied on STN can be written as the following nonautonomous system:

$$\frac{d\phi_p''(t)}{dt}=-2\gamma_p\phi_p'(t)-\gamma_p^2\phi_p(t)+\gamma_p^2\Gamma[V_p(t)], \quad (6)$$

$$\frac{dX''(t)}{dt}=abY(t)-(a+b)X'(t), \quad (7)$$

where

$$X(t) = [V_p(t), V_{d_1}(t), V_{d_2}(t), V_{g_1}(t), V_{d_2}(t), V_s(t), V_r(t), V_t(t)]^T, \tag{8}$$

$$Y(t) = \begin{pmatrix} \upsilon_{pp}\phi_p + \upsilon_{pi}\Gamma(V_p) + \upsilon_{pt}\Gamma(V_t) + \underline{\upsilon_{pg_2}\Gamma(V_{g_2})} - V_p(t) \\ \upsilon_{d_1p}\phi_p + \upsilon_{d_1d_1}\Gamma(V_{d_1}) + \upsilon_{d_1t}\Gamma(V_t) - V_{d_1}(t) \\ \upsilon_{d_2p}\phi_p + \upsilon_{d_2d_2}\Gamma(V_{d_2}) + \upsilon_{d_2t}\Gamma(V_t) - V_{d_2}(t) \\ \upsilon_{g_1d_1}\Gamma(V_{d_1}) + \upsilon_{g_1g_2}\Gamma(V_{g_2}) + \upsilon_{g_1s}\Gamma(V_s) - V_{g_1}(t) \\ \upsilon_{g_2d_2}\Gamma(V_{d_2}) + \upsilon_{g_2g_2}\Gamma(V_{g_2}) + \upsilon_{g_2s}\Gamma(V_s) - V_{g_2}(t) \\ \upsilon_{sp}\phi_p + \upsilon_{sg_2}\Gamma(V_{g_2}) + \underline{\underline{\upsilon_{ss}\Gamma(V_s)}} - V_s(t) + \underline{\upsilon_s\phi_{\mathrm{DBS}}(t)} \\ \upsilon_{rp}\phi_p + \upsilon_{rg_1}\Gamma(V_{g_1}) + \upsilon_{rt}\Gamma(V_t) - V_r(t) \\ \upsilon_{tp}\phi_p + \upsilon_{tg_1}\Gamma(V_{g_1}) + \upsilon_{tr}^A\Gamma(V_r) \\ +\upsilon_{tr}^B\Gamma[V_r(t-\tau)] - V_t(t) + \phi_n \end{pmatrix}. \tag{9}$$

Therein, the term with the single underline is introduced by Chen *et al.* in Ref. [11] based on Ref. [10]. The terms with double underline and wave line are introduced in this paper based on Ref. [11] to represent the ACS and CBBP DBS, respectively.

B. CBBP stimulation with interphase gap (IPG) setup

Charge injection from an electrode into the extracellular space is commonly controlled by one of three methods [48,49]: (i) the current-controlled method, i.e., a current source is attached between the WE and CE where a user-defined current is passed; (ii) the voltage-controlled method, i.e., current is driven between WE and CE, which refers to a third electrode; and (iii) the $V_{\mathrm{WE-CE}}$ controlled method, i.e., a voltage source is applied between WE and CE. The method used in this paper mainly refers to the third one, which is the simplest method to implement, where only the net potential between WE and CE needs to be controlled. What is more, voltage stimulation is most suitable for the case that the extracellular conductivity of neural tissue is unstable or the extracellular resistance is unrealistically high and may also change during the experiment [42,50,51].

The basic unit of stimulation with DBS is a brief and regularly repeating voltage difference between anode and cathode. This pulse is expressed as a rectangular waveform of adjustable amplitude (voltage: 0–1.25 V), duration (pulse width: 0–2.2 ms) and frequency (10–230 Hz). In particular, the four stimulation paradigms of CBBP can be computationally expressed as follows:

$$\phi_{\mathrm{DBS}}(t) = D_{\mathrm{S/AS}}(t), \tag{10}$$

where

$$D_{\mathrm{S}}(t) = \begin{cases} \delta & kT < |t| \leqslant kT + \delta \\ -\delta & kT + \delta + \mathrm{IPG} < |t| \leqslant kT + 2\delta + \mathrm{IPG} \\ 0 & \text{else} \end{cases} \tag{11}$$

and

$$D_{\mathrm{AS}}(t) = \begin{cases} \delta & kT < |t| \leqslant kT + \delta \\ 0 & kT + \delta < |t| \leqslant kT + \delta + \mathrm{IPG} \\ \frac{-\delta}{T-\delta-\mathrm{IPG}} & kT + \delta + \mathrm{IPG} < |t| \leqslant (k+1)T \end{cases} \tag{12}$$

represent the symmetric and asymmetric CBBP with IPG, respectively. T and δ is the period and duration of pulse current, $k \in \mathbb{N}$.

C. Simulation method and data analysis

The standard fourth-order Runge-Kutta integration scheme under the MATLAB simulating environment was employed with Eqs. (5)–(9). Following the previous studies [10,11], all simulations are performed up to 25 s with a fixed temporal resolution of 0.05 ms. The data in stable state from 5 to 25 s are used for statistical analysis. We perform the bifurcation and frequency analysis for several key parameters of the model to characterize the critical state transitions and neural oscillations. The bifurcation diagram is obtained by calculating the stable local minimum and maximum values of time series ϕ_p to identify the different dynamical state types. The power spectral density is estimated using the fast Fourier transform for the time series ϕ_p, the maximum peak frequency of which is defined as the dominant frequency of neural oscillations. The typical 2–4 Hz SWD oscillation region can be roughly outlined in the two-dimensional parameter space [e.g., see the region II in Fig. 3(a)], by combining the bifurcation and frequency analysis. To observe the control effect for SWD, the percentage of control for the SWD number is expressed as follows:

$$\eta = \frac{M(\mathrm{SWD}) - N(\mathrm{SWD})}{M(\mathrm{SWD})} \times 100. \tag{13}$$

Here, $M(\mathrm{SWD})$ represents the maximum of parametric grid points in the 2D parameter panel where the system showing SWD. Therein, the 2D parameter panel is covered by the uniformly fine-meshed $n \times n$ parametric grid points. In addition, $N(\mathrm{SWD})$ in this paper represents the SWD number

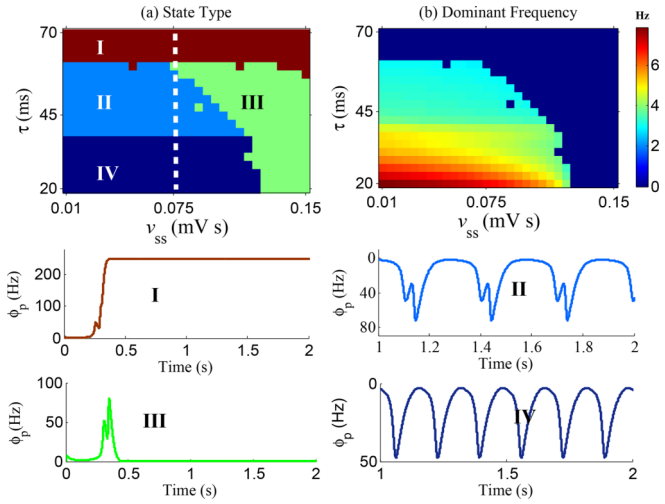

FIG. 3. Two-dimensional state analysis (a) and frequency analysis (b) in the (v_{ss}, τ) plane. (I) Saturation, (II) SWD, (III) low firing, (IV) simple oscillations. The parameters used are set as (similarly hereafter): $v_{pp} = 1$ mVs, $v_{pi} = -1.8$ mVs, $v_{rp} = 0.05$ mVs, $v_{rt} = 0.5$ mVs, $v_{tr}^{A} = v_{tr}^{B} = -0.8$ mVs, $v_{d_1p} = 1$ mVs, $v_{d_1d_1} = -0.2$ mVs, $v_{d_1t} = 0.1$ mVs, $v_{d_2p} = 0.7$ mVs, $v_{d_2d_2} = -0.3$ mVs, $v_{d_2t} = 0.05$ mVs, $v_{g_1d_1} = -0.1$ mVs, $v_{g_1g_2} = -0.03$ mVs, $v_{g_1s} = 0.3$ mVs, $v_{g_2d_2} = -0.3$ mVs, $v_{g_2g_2} = -0.075$ mVs, $v_{g_2s} = 0.45$ mVs, $v_{sg_2} = -0.04$ mVs, $v_{pt} = 1.8$ mVs $v_{pg_2} = -0.05$ mVs, $v_{tp} = 2.75$ mVs, $v_{sp} = 0.1$ mVs, $v_{tg_1} = v_{rg_1} = -0.035$ mVs. The parameters corresponding to the time series of four states in the lower panels are particularly taken as: (I) $\tau = 65$ ms, $v_{ss} = 0.05$ mVs; (II) $\tau = 45$ ms, $v_{ss} = 0.05$ mVs; (III) $\tau = 45$ ms, $v_{ss} = 0.14$ mVs, and (IV) $\tau = 25$ ms, $v_{ss} = 0.05$ mVs, respectively.

by the actions of the excessive autaptic excitation of STN or the external intervention (e.g., DBS). Hence, η represents the fraction of SWD abatements.

III. RESULTS

A. SWD abatement induced by the autaptic connections to STN through both the forward and backward pathways

Previous experimental and computational evidences have demonstrated that autaptic connections to typical nuclei of basal ganglia may be involved into the epileptogenesis mechanisms. In addition, modeling studies [10,11,22,52] have revealed that an excess of the slow dynamics of $GABA_B$ receptors in thalamic RE plays important roles in triggering both the onset and offset of absence seizures. To investigate the absence seizure activities induced by the slow kinetics of $GABA_B$ receptors in RE combined with the modulations of ACS, we focus on the parametric space (v_{ss}, τ), composed of the autaptic coupling and slow dynamic parameters. And then, both the bifurcation and frequency analysis are performed. As shown in Fig. 3(a), there are four types of dynamical states that appear in different parameter regions, that is (I) saturated state, (II) SWD discharges, (III) low firings, and (IV) simple oscillations (also see the lower panels of Fig. 3). When the inhibition projected from GPe to cortex is much less (e.g., $v_{pg_2} = 0.05$ mVs) and the $GABA_B$ delay is too long, the autaptic excitation of STN and inhibition from the RE have rather weak effects on TC neurons. Under these conditions, the recurrent excitation between the cerebral cortex and TC drives the firing of cortical pyramidal neurons to their saturation states in a short time (region I). For appropriate $GABA_B$ delay and the less v_{ss} (e.g., $v_{ss} <\approx 0.075$ mVs), STN has weak effect to cortex through the two pathways of forward STN → GPi → TC → PY projection and backward STN → GPe → PY projection. But, TC can be effectively suppressed at different time instants due to the independent mediation of $GABA_A$ and $GABA_B$ through RE-TC pathway. This can resultantly shape the firing of TC. When this effect propagates to the cortex, SWD oscillations are generated (region II). Compared to the Fig. 3(b), the frequency of SWD is within the 2-4Hz oscillations, which is consistent with the recorded EEG of patients with absence epilepsy. However, for the short $GABA_B$ delay, the interval between the two independent mediations of $GABA_A$ and $GABA_B$ is close enough to fuse these two signals together. This hence leads to the simple oscillation (region IV). For the large v_{ss}, it is noted that there exists competitive relations between inhibitions to TC through pathways of the GPi → TC and GPi → RE → TC. However, the inhibition of GPi → TC dominates due to the indirect modulation functions of GPi → RE. Therefore, we mainly consider the forward projection pathway of STN → GPi → TC → PY. As a result, as v_{ss} further increasing from $v_{ss} = 0.075$ mVs, the excessive excitation from STN can induce too much inhibitions to the cortex through the forward projection STN → GPi → TC → PY pathway [10] and the backward projection STN → GPe → PY pathway [11]. This ultimately push the system into the low firing state (region III).

B. Enhanced effect of backward projection pathway on the control of SWD number

In this section, we quantitatively investigate the effect of excessive v_{ss} on the control of SWD through the two types of forward and backward projection pathways (indicated by Refs. [10,11]). For illustration purposes, we estimate the state regions of absence seizures in the (v_{tp}, τ) panel. As disposed in Eq. (13), this panel is covered by $n \times n$ uniformly fine-meshed parametric grid points. Without loss of generality, in the following simulations, we always take $n = 10$. In particular, we count the number of parametric grid points, N(SWD), with which the system shows the SWD. Similar to previous result in Fig. 2 of Ref. [11], in Fig. 4(a), we reproduce the three types of dynamical states appear in different parameter regions (upper panel), i.e., saturation (I), SWD (II), and simple oscillations (IV), with fixing $v_{ss} = 0.04$ mVs, $v_{pg_2} = 0.05$ mVs, and $(v_{ss}, \tau) \in [1.8$ mVs, 3.2 mVs$] \times [20$ ms, 70 ms$]$, respectively. It is clearly seen that the weak autaptic excitations of STN can not push the system to the low firing state. However, as shown in the lower panel of Fig. 4(a), the excessive autaptic excitations of STN (e.g., $v_{ss} = 0.1$ mVs) can induce the low firings (region III). This is due to the double inhibitory suppressions from the forward and backward projection pathways.

In Fig. 4(b), we systematically give the percentages of control for the SWD number with v_{ss} continuously increasing from 0.075 to 0.15 mVs. According to Eq. (13), M(SWD)

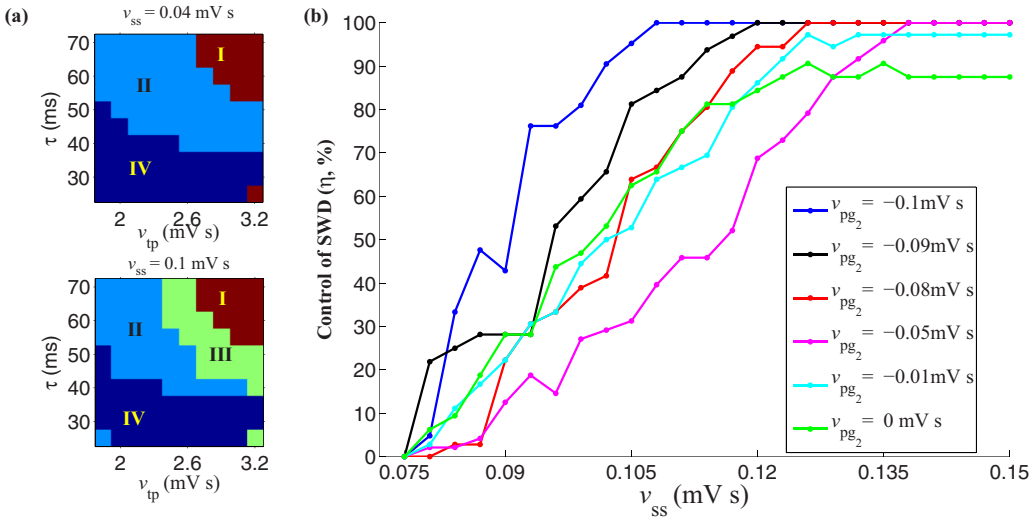

FIG. 4. (a) Two-dimensional state analysis in the (v_{tp}, τ) plane with $v_{ss} = 0.04$ mVs (upper panel) and $v_{ss} = 0.1$ mVs (lower panel), respectively. (I) saturation, (II) SWD, (III) low firing, (IV) simple oscillations. (b) The effect of v_{ss} on the percentage of control for SWD regulated by the v_{pg_2}.

here represents the maximum of parametric grid points showing SWD in the (v_{ss}, τ) panel. In particular, M(SWD) is calculated by fixing $v_{ss} = 0.075$ mVs, which cannot drive the SWD into low firing. In contrast, N(SWD) represents the SWD number at various values of v_{ss} when the excessive autaptic excitation of STN takes effect on the system. Then η represents the fraction of successful inhibitions of SWD into low firings. As shown with pink break line in Fig. 4(b), we fixed $v_{pg_2} = 0.05$ mVs keeping the backward projection STN → GPe → PY pathway effective in control SWD. It is clearly seen that with v_{ss} gradually increasing, the SWD is gradually controlled under the functions of both the forward and backward projection pathways. In particular, as $v_{ss} = 0.138$ mVs, the excessive autaptic excitation of STN can totally drive the system from SWD into the low firing. That is, the absence seizures have been fully abated. To verify that the backward projection pathway is reliably to take effects for the control of SWD, we particularly set $v_{pg_2} = 0$ mVs (green line), i.e., fully interdicting the inhibition of backward projection pathway. Compared to pink line, the green line clearly shows that ultimately the SWD can not completely controlled (about ten percent remained) due to the single pathway control effect of the forward projection. On the other hand, as indicated by blue break line, for the stronger inhibitory projection from GPe to PY, the SWD can be relatively easier fully controlled at $v_{ss} = 0.108$ mVs.

C. Bidirectional modulation of S-CBBP-IPG stimulation frequency on the number of SWD

STN has been demonstrated to be involved into the occurrences and abatements of absence seizures. In particular, it is found that the membrane excitability in the subthalamic nucleus (STN) neurons can be changed by the deep brain stimulation (DBS) applied through a concentric bipolar electrode inserted into the STN [13,36]. Hence, in this section we investigate the control effect of STN DBS with different stimulation parameters on absence seizures under the modulations of autaptic connection to STN. According to the experimental setting of Ref. [36], symmetric charge balanced biphasic pulse DBS with fixing inter-phase gap (S-CBBP-IPGx, $x = T - 2\delta$) is considered in this section. Note that the periodical switch between positive and negative pulses of CBBP-DBS stimulations to STN can result in the recurrent oscillations of membrane excitability of STN neurons. In most therapeutic DBS conditions, rectangular monophasic voltage pulses of adjustable amplitude (1–10 V), duration (0.06–0.45 ms) and pulse rate (2–250 pulses per second) are used [42,48,53]. However, in this paper, to decrease the side effects of overhigh currents to the brain, as a compromise we increase the pulse duration (i.e., 1.2–2 ms) to reduce the stimulation amplitude. As shown in Figs. 5a$_1$, 5a$_2$, the relatively weak stimulation amplitude of 0.1–1.25 V can generate significant effect on SWD occurrence. In addition, we fix the pulse frequency within 10–230 Hz. During the simulations, stimulus trains were made by the Eqs. (10)–(12) [see also the Fig. 2(d)]. As shown in Fig. 5, we evaluate the effects of stimulation strength (Figs. 5a$_1$, 5a$_2$), pulse duration (Figs. 5b$_1$, 5b$_2$), and stimulation frequency (Figs. 5c$_1$, 5c$_2$) of STN S-CBBP DBS on the absence seizures. Responses to both the ACS and STN S-CBBP DBS are examined in the panels of (v_{ss}, A), (v_{ss}, δ), and (v_{ss}, f), respectively.

It is seen from Figs. 5a$_1$, 5a$_2$ that for the weak autaptic strength, the total number of SWD occurrences was high around 50 and only high stimulation amplitude can eventually decrease the SWD occurrences. With the autaptic function increasing, for example, $v_{ss} = 0.05$ mVs, the number of SWD can be gradually abated with the stimulation amplitude (SA) being augmented from lower SA values. In particular, 1 V of SA can completely control SWD. Similar results can also be observed in Figs. 5b$_1$, 5b$_2$ where we stimulated the STN with 1.2 to 2 ms of stimulation pulse duration (SD) as well as 1 V and 100 Hz of SA and stimulation frequency (SF), respectively. It clearly indicates that under the weaker modulation of autaptic functions, SWD occurrence can be enhanced during low SD stimulations but gradually suppressed during

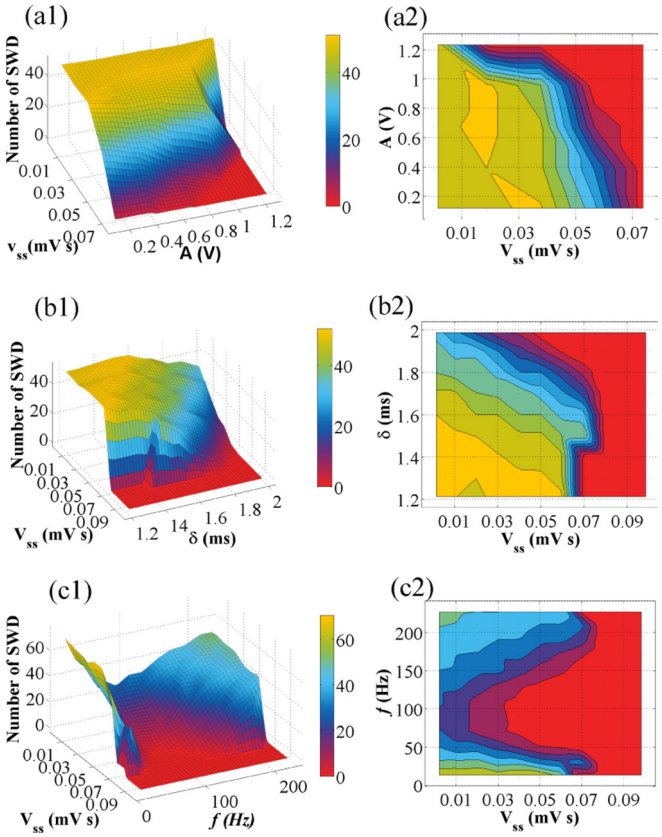

FIG. 5. Evolutions of SWD number (left panel) and the corresponding contour plots (right panels) driven by both the autaptic connection strength of STN, v_{ss}, and the parameters of STN CBBP stimulation, i.e., stimulation amplitude (A, a1 and a2), pulse duration (δ, b1 and b2), and stimulation frequency (f, c1 and c2), with fixing ($f = 100$ Hz, $\delta = 2$ ms), ($A = 1$ V, $f = 100$ Hz) and ($\delta = 2$ ms, $A = 1$ V), respectively.

high SD stimulations. In addition, previous studies have suggested that DBS effects depend on the stimulus frequency employed [13,36,54]. To investigate the sensitivity of STN to the stimulation frequency, we applied S-CBBP DBS to STN at different stimulus frequencies in Fig. 5c$_1$, 5c$_2$ with autaptic modulations. It is clear seen that under the moderate autaptic modulation both the low frequency (e.g., <50 Hz) and high frequency (e.g., >150 Hz) stimulations enhance SWD occurrence, while the moderate frequency stimulation decreases the number of SWD occurrences. In particular, the number of SWD occurrence can be largely controlled using the stimulation with around the 100 Hz of frequency. This result indicates that stimulation in frequency-dependent manner can bidirectionally modulate the SWD occurrence. Briefly, this is because low frequency stimulation can not affect the intrinsic activity of STN neurons. As the stimulation frequency increases, it is superposed to enhance both the intrinsic activity of STN neurons and the transmission of the neural activity [54], which then further abates the SWD through both the forward and backward projection pathways of STN. However, with the frequency further getting larger and larger, the number of SWD gradually increases back again due to that the high frequency stimulation can mask the intrinsic activity of STN [54], which leads to an informational lesion and weakens the control effect of DBS.

To further evaluate the beneficial effects of typical stimulation frequency on the control of SWD number, we first stimulate the STN with the fixed pulse duration of 2 ms, as well as the incrementally increased stimulation amplitude (SA = 0.7, 0.75, 0.8, 0.85, and 0.9 ms) and stimulation frequency (SF = 40, 70, 100, and 130 Hz) in Fig. 6(a). The statistic result also shows that SWD occurrence is gradually suppressed when the SA increases from 0.7 to 0.9 V. However, it is clearly seen that the SWD number is significantly smaller at moderate frequency stimulations (i.e., 70 Hz and 100 Hz) than that of both the low frequency (40 Hz) and high-frequency (130 Hz) stimulations. That means the control effect of SWD is particularly frequency-dependent. Thereby, we then stimulate the STN with the fixed frequency of 100 Hz, to observe the effect of the incrementally increased stimulation pulse duration (SD = 1.1, 1.5, 1.8, 2, and 2.2 ms) and stimulation amplitude (SA = 0.8, 1, and 1.2 V) in Fig. 6(b). It clearly indicates that SWD occurrence is gradually suppressed when the SD changes from 1.1 to 2.2 ms. Also of note, the larger SA is more easily suppress the occurrence of SWD. In particular, as shown in Fig. 6(c), when we stimulate the STN with the fixed SA of 0.8V, as well as the incrementally increased pulse duration (SD = 1.8, 2, and 2.2 ms) and stimulation frequency (SF = 40, 70, 100, 130, and 160 Hz), the number of SWD first descends then rises with SF increasing. The smallest number of SWD is obtained at both the 70 and 100 Hz frequency stimulations. This means that the SWD occurrence is firstly suppressed and then enhanced with the SF incrementally increasing, which implies that the SWD occurrence can be bidirectionally modulated. In particular, the bidirectional modulating effects can be further improved with SD incrementally increasing. Finally, to examine the contribution of autaptic functions to the control effect of DBS on SWD, we fix $\delta = 2$ ms from Fig. 6(c) (corresponding to the red line in Fig. 6(d) with $v_{ss} = 0.05$ mVs), and additionally incrementally increase v_{ss} in Fig. 6(d) (0.01, 0.03, 0.05, and 0.07 mVs). It is obviously observed that the control effect of DBS on SWD can also be significantly further improved at the 70 and 100 Hz frequency stimulations.

In sum, these results suggest that STN is involved in maintaining the rhythmic activity of SWD through changing the STN activity using both the autaptic and DBS modulations.

D. Control effect of CBBP DBS IPG on the number of SWD

Most experimental studies have investigated the effect of pulse shapes on stimulus efficacy [42,55,56]. It is particularly shown that adding an IPG between the leading and the lagging phase of CBBP DBS significantly increased the stimulus efficacy, compared to the case that lack an IPG [42]. In addition, they also found that symmetrical CBBP DBS with IPG (S-CBBP-IPGx) is more effective than asymmetrical CBBP DBS with IPG (AS-CBBP-IPGx). Therefore, S-CBBP-IPGx is appealing for DBS. To explore whether these stimulation strategies are still valid in controlling absence seizures, in this section we set out to compare the effects of two types of AS-CBBP-IPGx and S-CBBP-IPGx stimulations on the SWD number evolutions. We particularly set the value

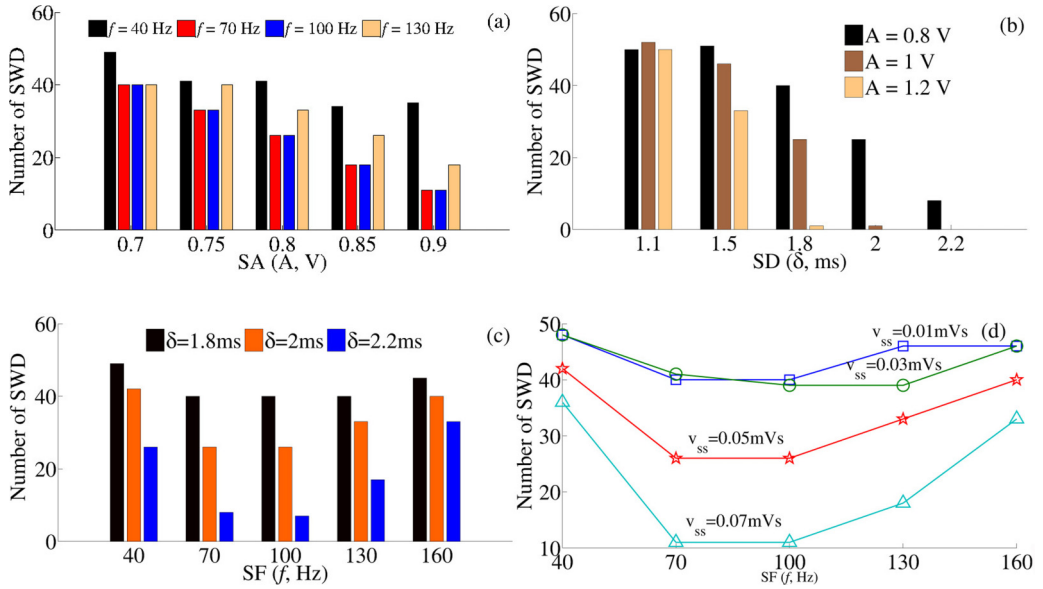

FIG. 6. The STN S-CBBP-IPGx DBS effects on the number of SWD by changing the various stimulation parameters with fixing $\delta = 2$ ms (a), $f = 100$ Hz (b) and $A = 0.8$ V (c), respectively. (d) The effect of stimulation frequency (SF) on the number of SWD, where $\delta = 2$ ms, $A = 0.8$ V, and $v_{ss} = 0.01$ mVs, 0.03 mVs, 0.05 mVs, and 0.07 mVs, respectively.

of IPG, i.e., x, incrementally increase from 0 to 6 ms and decrementally decrease from 6 to 0 ms, respectively. Statistical analysis in Fig. 7 clearly indicates that the responses to AS-CBBP-IPGx and S-CBBP-IPGx stimulations are qualitatively same. That is CBBP DBS with no and large IPG can enhance the SWD occurrence, while the moderate IPG (e.g., IPG = 2, 3, and 4 ms) can effectively suppress the SWD occurrence. In particular, the stronger autaptic functions can further improve the SWD control effect of CBBP-IPGx stimulations. However, on the whole, AS-CBBP-IPGx is significantly less beneficial than S-CBBP-IPGx. These results are consistent with the responses to two types of AS-CBBP-IPGx and S-CBBP-IPGx stimulations employed in the previous experimental models.

IV. CONCLUSION

Based on a modified basal ganglia–corticothalamic (MBGCT) network model, we have computationally examined the involvement of STN in modulating SWD occurrence using the methods of autaptic connection to STN (ACS) and STN DBS. Results showed that the strong ACS can effectively control SWD occurrence, while the weak ACS, even though having no effect in itself on SWD suppression, could reduce the DBS intensity to basically induce the same efficacy. Also, results demonstrated the experimental findings that stimulation in frequency-dependent manner can bidirectionally modulate the SWD occurrence. Furthermore, we investigated the effect of CBBP-DBS shapes, i.e., AS-CBBP-IPGx and S-CBBP-IPGx stimulations, on SWD occurrence under the weak modulation of ACS. It is shown that CBBP DBS with the moderate IPG (e.g., IPG = 2, 3, and 4 ms) can effectively suppress the SWD occurrence. However, AS-CBBP-IPGx is significantly less beneficial than S-CBBP-IPGx. These results are basically consistent with the previous experimental findings. Our work, on the other hand, supports the idea that the STN is involved in the maintenance mechanism of SWD occurrence. This might offer a clue for uncovering the mechanism underlying STN DBS for treatment of absence seizures. Hopefully, this work is helpful in finding the best compromise between clinical effect and power consumption as well as the potentially reduced side effects of the stimulus generator, and eventually provides testable hypotheses for future clinical research.

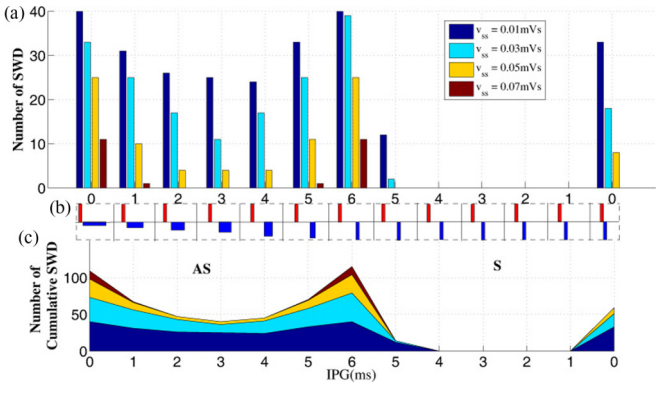

FIG. 7. The effect of IPG of CBBP stimulations on the number of SWD. Stimulation amplitude is 0.8V, stimulation frequency $f = 100$ Hz, the duration of leading phase is 2 ms.

ACKNOWLEDGMENTS

This work was supported by the National Natural Science Foundation of China (Grants No. 11702018 and No. 11772019), the National Key R&D Program of China (Grant No. 2017YFF0207401), the Project funded by China Postdoctoral Science Foundation (Grants No. 2016M600037 and No. 2018T110043), and the Fundamental Research Funds for the Central Universities (Grant No. FRF-TP-16-068A1).

[1] C. Panayiotopoulos, Epilepsia **49**, 2131 (2008).
[2] H. Meeren *et al.*, J. Neurosci. **22**, 1480 (2002).
[3] V. Crunelli and N. Leresche, Nat. Rev. Neurosci. **3**, 371 (2002).
[4] H. Blumenfeld and K. Meador, Epilepsia **55**, 1145 (2014).
[5] E. Sitnikova *et al.*, Brain Res. **1543**, 290 (2014).
[6] A. Kandel and G. Buzsaki, J. Neurosci. **17**, 6783 (1997).
[7] H. Meeren *et al.*, Exp. Neurol. **217**, 25 (2009).
[8] E. Sitnikova *et al.*, Brain Res. Bull. **120**, 106 (2016).
[9] C. Deransart *et al.*, Epilepsy Res. **32**, 213 (1998).
[10] M. Chen *et al.*, PLoS Comput. Biol. **10**, e1003495 (2014).
[11] M. Chen *et al.*, PLoS Comput. Biol. **11**, e1004539 (2015).
[12] B. Hu *et al.*, Chaos Soliton. Fract. **95**, 65 (2017).
[13] D. Kase, T. Inoue, and K. Imoto, J. Neurophysiol. **107**, 393 (2011).
[14] P. Suffczynski, S. Kalitzin, and F. Lopes da Silva, Neuroscience **126**, 467 (2004).
[15] G. Baier *et al.*, Front. Physiol. **3**, 281 (2012).
[16] M. Breakspear *et al.*, Cereb. Cortex **16**, 1296 (2005).
[17] D. Fan *et al.*, J. Computat. Neurosci. **43**, 203 (2017).
[18] D. P. Yang and P. A. Robinson, Phys. Rev. E **95**, 042410 (2017).
[19] Y. Kim, J. Korean Phys. Soc. **71**, 63 (2017).
[20] L. Wiles *et al.*, Sci. Rep. **7**, 44006 (2017).
[21] Y. Xu *et al.*, Sci. Rep. **7**, 43452 (2017).
[22] D. Guo *et al.*, in *Proceedings of the In ternational Conference on Neural Information Processing* (Springer, Cham, 2017), p. 613.
[23] G. Tamas, E. Buhl, and P. Somogyi, J. Neurosci. **17**, 6352 (1997).
[24] J. Lubke *et al.*, J. Neurosci. **16**, 3209 (1996).
[25] S. Cobb *et al.*, Neuroscience **79**, 629 (1997).
[26] A. Bacci *et al.*, J. Neurosci. **23**, 9664 (2003).
[27] W. Theodore and R. Fisher, Lancet Neurol. **3**, 111 (2004).
[28] A. Valentin *et al.*, Epilepsia **54**, 1823 (2013).
[29] C. Heck *et al.*, Epilepsia **55**, 432 (2014).
[30] N. Usui *et al.*, J. Neurosurg. **102**, 1122 (2005).
[31] S. Ahn *et al.*, Front. Computat. Neurosci. **11**, 39 (2017).
[32] Z. Wang and Q. Wang, Front. Computat. Neurosci. **11**, 22 (2017).
[33] B. Rosin *et al.*, Neuron **72**, 370 (2011).
[34] H. Zhang, Q. Wang, and G. Chen, Chaos **24**, 033134 (2014).
[35] D. Fan, Z. Wang, and Q. Wang, Commun. Nonlinear Sci. Numer. Simulat. **36**, 219 (2016).
[36] S. Chabardes *et al.*, Epileptic Disord. **4**, 83 (2002).
[37] B. Hu *et al.*, Cogn. Neurodyn. **12**, 103 (2018).
[38] L. Vercueil *et al.*, Epilepsy Res. **31**, 39 (1998).
[39] C. Pantoja-Jimenez *et al.*, Brain Stimul. **7**, 587 (2014).
[40] J. Vesper *et al.*, Epilepsia **48**, 1984 (2007).
[41] I. Osorio *et al.*, Epilepsia **48**, 1561 (2007).
[42] N. Cappaert *et al.*, Int. J. Neural Syst. **23**, 1250031 (2013).
[43] S. N. Ching, E. N. Brown, and M. A. Kramer, Phys. Rev. E **86**, 021920 (2012).
[44] D. Breuer, M. Timme, and R.-M. Memmesheimer, Phys. Rev. X **4**, 011053 (2014).
[45] F. Farkhooi and W. Stannat, Phys. Rev. Lett. **119**, 208301 (2017).
[46] M. diVolo, R. Burioni, M. Casartelli, R. Livi, and A. Vezzani, Phys. Rev. E **93**, 012305 (2016).
[47] J. Zierenberg, J. Wilting, and V. Priesemann, Phys. Rev. X **8**, 031018 (2018).
[48] D. Merrill, M. Bikson, and J. Jefferys, J. Neurosci. Meth. **141**, 171 (2005).
[49] D. Hardesty and H. Sackeim, Biol. Psychiat. **61**, 831 (2007).
[50] P. Jayakar, Adv. Neurol. **63**, 17 (1993).
[51] S. Miocinovic *et al.*, Exp. Neurol. **216**, 166 (2009).
[52] A. Destexhe, J. Neurosci. **18**, 9099 (1998).
[53] C. C. Mclntyre *et al.*, J. Clin. Neurophysiol. **21**, 40 (2004).
[54] W. Grill, A. Snyder, and S. Miocinovic, Neuroreport **15**, 1137 (2004).
[55] R. Shepherd and E. Javel, Hear. Res. **130**, 171 (1999).
[56] C. van den Honert and J. Mortimer, Ann. Biomed. Eng. **7**, 117 (1979).